MESO-NANO AND MICRO-NANO ION TRANSPORT IN POROUS CARBON COMPOSITE ELECTRODES FOR ENERGY STORAGE APPLICATIONS

C.Lekakou[1], F.Markoulidis[1], C.Lei[1], A.Sorniotti[1], J.Perry[2], C.Hoy[2], B.Martorana[3], I.Cannavaro[3], M.Gosso[3]

[1]*Division of Mechanical, Medical and Aerospace Engineering, University of Surrey, Guildford, Surrey GU2 7XH, UK*
[2]*AGM Batteries Ltd., Thurso Business Park, Thurso, Caithness, KW14 7XW, UK*
[3]*Centro Ricerche Fiat S.C.p.A., Strada Torino 50, 10043 Orbassano (TO), Italy*
**e-mail address of the corresponding author: C.Lekakou@surrey.ac.uk*

Keywords: supercapacitors, electrolyte, modelling, ion transport

Abstract
In energy storage devices carbonaceous composite electrodes are a popular choice, consisting of activated carbon (ac), conductive additives and a polymeric binder matrix. The active electrode components are in the form of ac particles, ac fibres, or ac monolith combined with conductive additives such as carbon black. Activated carbon plays the most important role for storing a large amount of energy in the form of ions contained in the carbon nanopores. This study considers a modelling approach to the meso-nano and micro-nano infiltration of ions into the porous carbon structure during the operation of the energy storage device. Depending on the pore size, ion size and solvent molecule size, ions may be solvated or unsolvated as they move, where ions are solvated in meso-pores for most cases. Molecular model simulations have been performed to determine the values of the geometrical parameters of different ions, solvated and unsolvated in various solvents. A meso-nano and micro-nano ion infiltration model has been developed in this study under both steady state and dynamic conditions.

1 Introduction
Electrochemical double layer capacitors (EDLCs) and other energy storage devices are based on the concept of large pore surface area to increase the distributed charge. However, such pore area needs to be accessible to the ions of the electrolyte under the operating conditions. Apart from the average parameters, pore size distribution is very important with relation to energy storage and power performance. First of all, in terms of capacitance the pore size needs to be sufficiently large for the ions to be able to enter the pore and travel within it. While this is the minimum requirement, different pore sizes favour capacitance in different ways, depending on how large surface area they offer for ion adsorption and how much area of Stern layer they can pack [1,2]. Furthermore, the effects of pore size distribution become more pronounced under transient conditions.

Modelling of ion transport through porous materials is very important for the understanding of processes and optimization of materials structure and behaviour for a number of

applications including supercapacitors, batteries, desalination, fuel cells, and hydrogen storage. The task has been undertaken with great enthusiasm by electrochemists whose models are based on electrochemical and thermodynamic principles which are subsequently translated to equivalent electrical circuit models for which in practice is almost impossible to determine the full set of parameters. As a result these models cannot at present be applied to a real material, which greatly limits their usefulness as a material design tool.

If in this study it is assumed that there are no faradaic reactions (which occur in the case of batteries, for example, but are absent in other devices such as EDLC supercapacitors), the Stern or Helmholtz or inner layer by the solid surface of the pore in contact with the electrolyte is the most important region of the electrolyte with the highest voltage gradient which controls the adsorption or de-adsorption of ions at the solid surface of electrode during the charge and discharge phase, respectively. The thickness of the Stern layer is of the order of the corresponding solvated electrolyte ion [3]. The next layer with voltage gradient, although not as large voltage gradient as in the Stern layer, is the stagnant diffusion layer the boundary of which is the slip plane at which the potential is equal to the ion zeta potential. Finally, the rest of the solution in the pore is considered as bulk solution extending until the potential is zero at the Debye length which is related to the ionic strength of the electrolyte.

The aim of this study is to model the effects of a multi-pore size distribution on the capacitance, the energy storage and the power of a porous device under different charge-discharge rates, so that effective porous electrodes can be designed and fabricated with pores accessible to the ions under different conditions of operation. According to Huang et al [4] three ranges of nano-pore sizes have been considered with distinct capacitance models: micro-pores, meso-pores and macro-pores. The present study includes modelling under steady state and dynamic ion transport conditions.

2. Steady state ion transport and capacitance models

In the model where it is assumed that ion transport has reached steady state, the following equation applies for the charge q of each type of ion:

$$\nabla^2 q = 0 \tag{1}$$

Huang et al [4] distinguished between three types of pore sizes d_p: micro-pores with $d_p < 2$ nm, meso-pores with 2 nm $< d_p <$ 50 nm, and macro-pores with $d_p >$ 50 nm. In this study, the pore size limits are given by the parameters of the physicochemical modeling, as follows: micro-pores with $d_p \leq 2d_{solvated\ ion}$, meso-pores with $2d_{solvated\ ion} < d_p < L_{Stern}+L_{SDL}$, and macro-pores with $d_p \geq L_{Stern}+L_{SDL,}$ where L_{Stern} and L_{SDL} are the thickness of the Stern and the stagnant diffuse layer respectively. In all these cases the steady state ion transport equation (1) is applied and integrated analytically to derive the capacitance.

For the micro-pores ($d_p \leq 2d_{solvated\ ion}$), equation (1) is applied in cylindrical coordinates and integrated to yield:

$$C = \frac{2\varepsilon_r \varepsilon_o A}{d_p \ln\left(\frac{d_p}{d_{solvated\ ion}}\right)} \tag{2}$$

Where C is the capacitance, A is the area of the electrode, ε_r is the dielectric constant of the electrolyte medium, and ε_o is the vacuum permittivity.

For the meso-pores ($2d_{solvated\ ion} < d_p < L_{Stern}+L_{SDL}$), equation (1) is also applied in cylindrical coordinates and integrated to yield:

$$C = \frac{2\varepsilon_r\varepsilon_o A}{d_p \ln\left(\frac{d_p}{(d_p - d_{solvated\ ion})}\right)} \quad (3)$$

For the macro-pores ($d_p \geq L_{Stern}+L_{SDL}$), the electrode surface can be assumed to be flat and equation (1) is applied in Cartesian coordinates and integrated to yield:

$$C = \frac{\varepsilon_r\varepsilon_o A}{L_{Stern}} \quad (4)$$

3. Results of electrode capacitance in steady state ion transport

The first task has been to determine the diameter of the solvated ion, which is considered to be the limiting size of the solvated ion. Furthermore, the maximum capacitance for very small pores could be related to the adsorption of the unsolvated ion which may also result in deformation of the pore walls. Molecular modeling was carried out for this purpose using Materials Studio v5.0. Figure 1(a) presents the predicted TEA^+ ion solvated in propylene carbonate (PC): This gives a smaller diameter, which is the limiting size, $d_{TEA/PC}$ = 1.28 nm. The minimum electrode pore size that can possibly be used for the transport and adsorption of TEA^+ is $d_{p,min}$=0.67 nm when the ion is in its unsolvated state and can possibly deform the pore, as it is presented in Figure 1(b). The anion BF_4^- is a smaller ion, with a solvated ion size of $d_{BF4/PC}$ = 0.45 nm (see Figure 2), so its transport is not the control mechanism for the electrode capacitance and all the focus is on the bigger cation TEA^+.

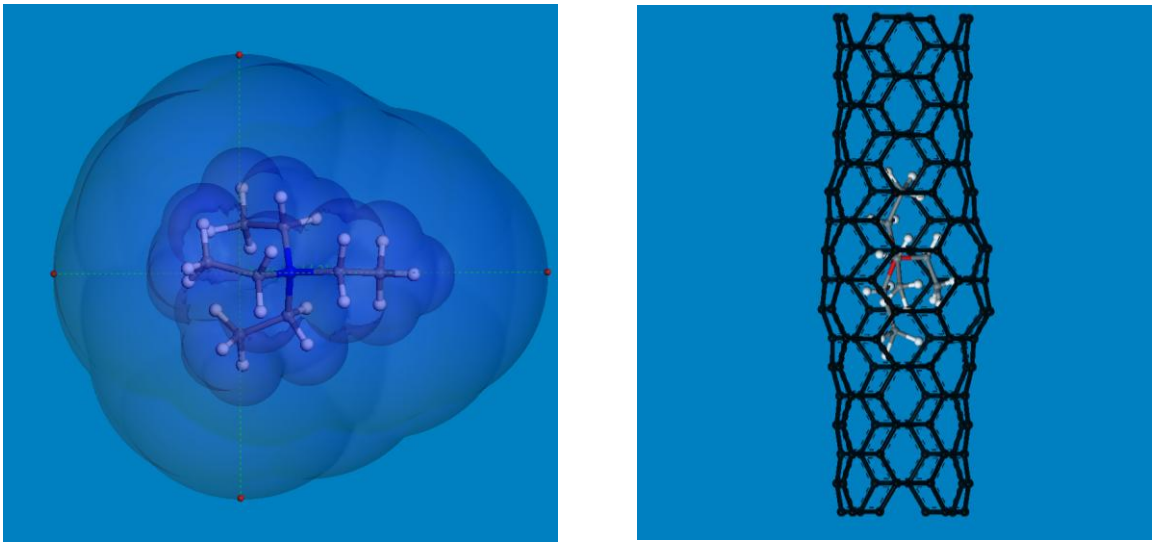

(a) (b)

Figure 1. (a) Predictions of TEA^+ ion solvated in propylene carbonate (PC); (b) predictions of unsolvated TEA^+ ion in a deformed carbon pore.

The model was applied to activated carbon electrodes coated with 5 wt% PVDF on aluminium foil and tested in an electrochemical double layer capacitor (EDLC) cell with 1 M $TEABF_4$/PC electrolyte. Figure 3 presents an SEM micrograph and the BJH pore size distribution of the coated electrode. Figure 4(a) presents the Nyquist plot of measurements for the capacitor cell from which it can be determined that the electrode capacitance is C = 92

F/g at 10 mHz. Figure 4(b) presents the predicted capacitance as a function of the pore diameter according to the capacitance models presented in section 2, based on steady state ion transport. The predictions give an average electrode capacitance of 92 F/g, taking into account the pore size distribution from Figure 3(b). It can be seen that there is excellent agreement between experiment and model predictions, where the experimental capacitance value has been provided by the very low frequency data of the Nyquist plot in Figure 4(a).

Figure 2. Predictions of BF_4^- ion solvated in propylene carbonate (PC)

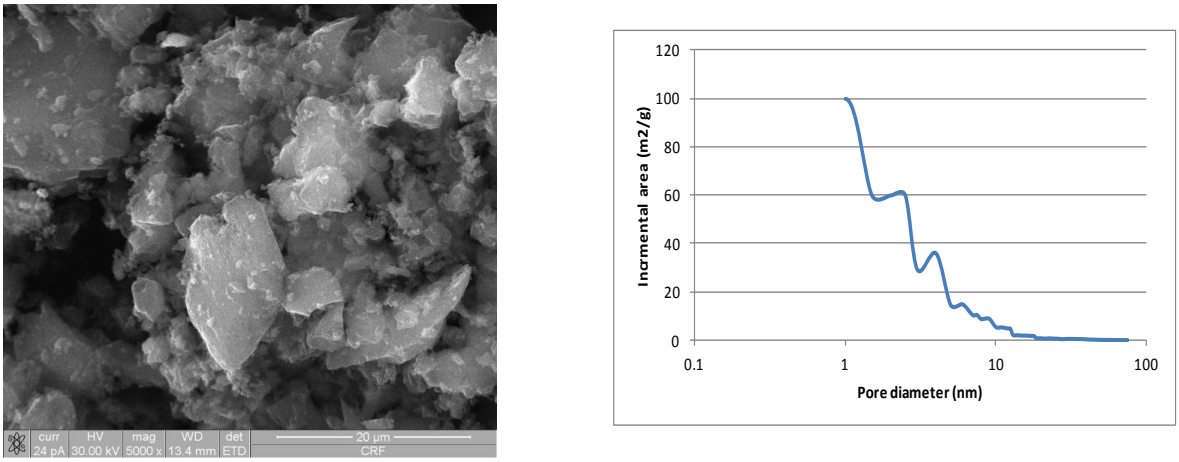

Figure 3. SEM of AC powder and pore size distribution of the electrode coating

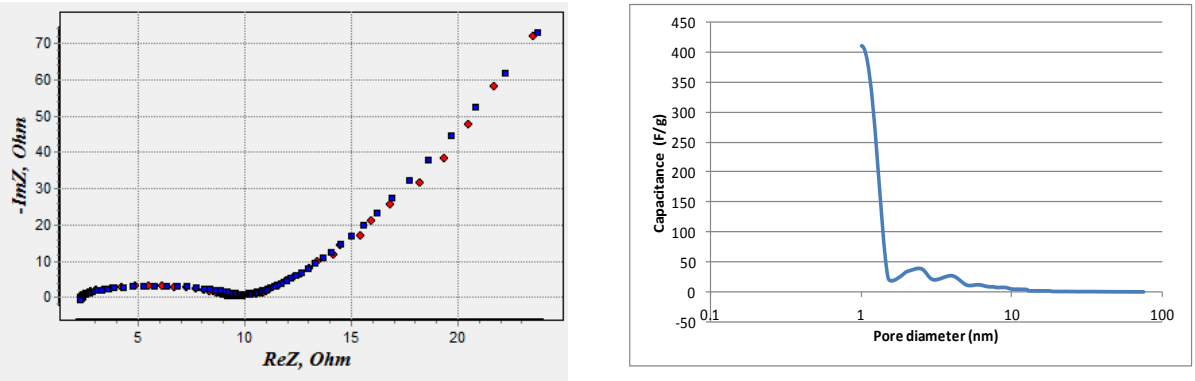

Figure 4. (a) Nyquist plot of the AC-based capacitor cell with electrolyte 1 M $TEABF_4$/PC from electrochemical impedance spectroscopy measurements; (b) predicted electrode capacitance as a function of the pore diameter using the capacitance models based on steady state ion transport.

The next step has been to consider an ionic liquid electrolyte which operates without a solvent, for example the EMI-TFSI electrolyte. Figure 5 shows the molecular modeling of the Van der Waals volume of the cation EMI^+ and anion $TFSI^-$. The two ions are of very similar size, 1.01 and 1.00 nm maximum length and minimum length d_{EMI} = 0.62 nm and d_{TFSI} = 0.60 nm, respectively, where their minimum length is the limiting size in the ion transport through the pores.

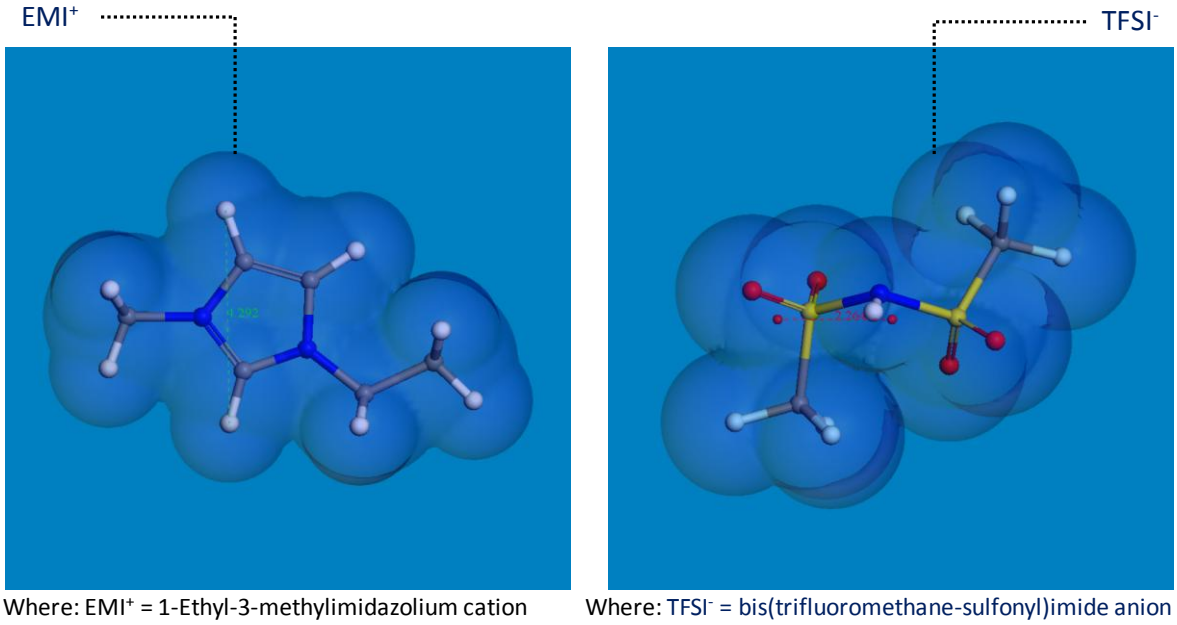

Figure 5. Predictions of EMI^+ ion and $TFSI^-$ ion of the EMI-TFSI ionic liquid electrolyte

Table 1. Predictions and experimental data of electrode capacitance for electrolyte EMI-TFSI, where the experimental data are from Lazzari [5]

AC type [5]	Pore Dia (nm) [5]		Predicted C (F/g)	Experimental C (F/g) [5]
CA1	6		53	52
CRFB4	9		56	52
CRFB5	20		103	61
CRFC5	15		92	56
X1a	6		153	90
X2a	14		175	106
X3a	15		240	125
AC	2.7		69	109
ACT	2.7		66	85
DTC8	3.3		58	107

Lazzari [5] manufactured a large range of activated carbon aerogels and xerogels which he incorporated in supercapacitor cells with ionic liquid electrolytes and tested in cyclic voltametry at 0.02 V/s in the range of -2.1V/ -0.2V versus Fc/Fc^+. He also characterized the electrode materials in terms of pore size distribution in the range 1-100 nm. As a result, he has tables of experimental data with porosity, mean pore diameter and electrode capacitance (mean integral value from the CV test) for all his activated carbons. In the present study, we used the values of his mean pore diameter and applied them to the appropriate capacitance

models under steady state ion transport for the EMI-TFSI electrolyte. The predicted electrode capacitance for his various activated carbons is presented in Table 1 and also compared with the experimental data. It can be seen that the predictions sometimes agree well but other times disagree with the experimental data; the reason for the latter is thought to be that in this case the model did not consider the full pore size distribution. It might also be that dynamic effects are present.

4. Dynamic charge transport model

While the predicted electrode capacitance for activated carbon and 1 M $TEABF_4$/PC electrolyte in section 3 agreed with the experimental capacitance value obtained at 10 mHz, the capacitance obtained at different charge-discharge rates is not constant as can be seen in Figure 6. Hence, it is clear that dynamic effects are important in the ion transport model and a dynamic charge transport model is presented in this study based on a phenomenological model of the electrode-electrolyte system.

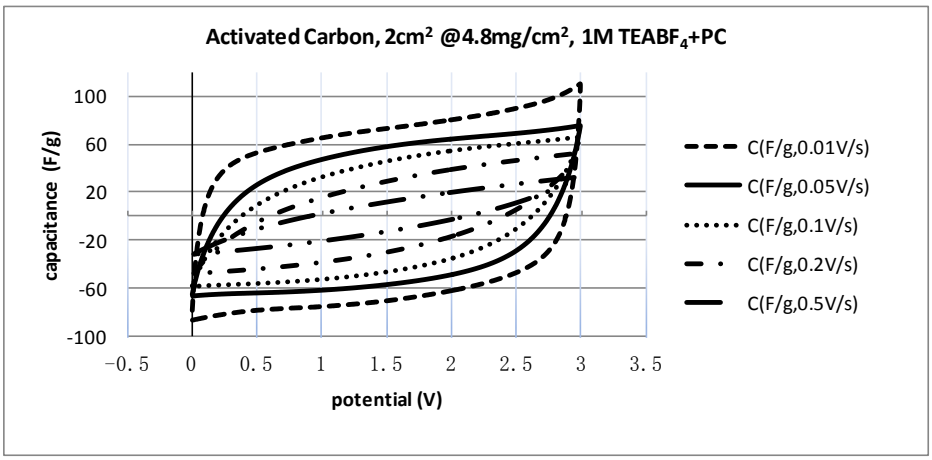

Figure 6. Cyclic voltammetry of a capacitor cell at different rates

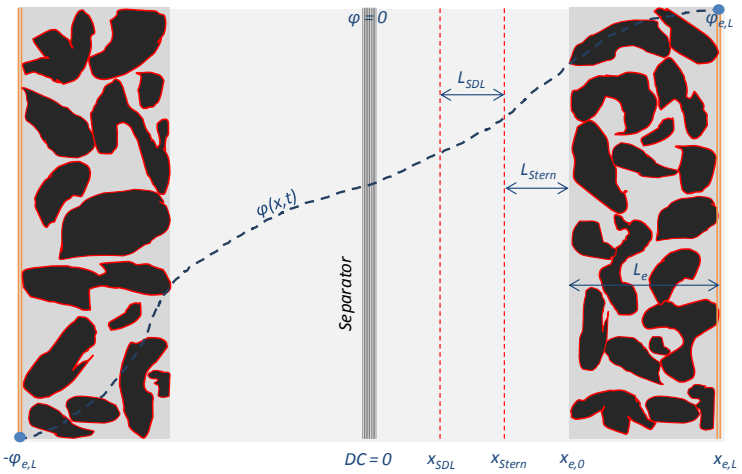

Figure 7. Schematic diagram of the ion transport and charge distribution model for porous electrodes and foil current colectors

Figure 7 presents the schematic of the porous electrode-electrolyte system considered in the dynamic charge transport model of this study. The rate of accumulation of charge in the

current collector at $x_{e,L}$ during charge or loss of charge in the current collector during discharge is given by the equation:

$$\frac{dq_{e,L}(t)}{dt} = J_{q_{C,L}}(t)\left(\frac{\varepsilon_{carbon}}{R_{C\text{-}Al}}\right) + J_{q_{sol,L}}(t)\left(\frac{\varepsilon_{sol}}{R_{sol\text{-}Al}}\right) + J_{q_{SDL,L}}(t)\left(\frac{\varepsilon_{SDL}}{R_{SDL\text{-}Al}}\right) + J_{q_{Stern,L}}(t)\left(\frac{\varepsilon_{Stern}}{R_{Stern\text{-}Al}}\right) \quad (5)$$

where J denotes charge flux through a surface, including the total contact surface C-L between carbon and the outer electrode, the total contact surface Stern-L between the Stern layer and the outer electrode, the total contact surface SDL-L between the stagnant diffusion layer and the outer electrode, and the total contact surface sol-L between the bulk solution and the outer electrode; also ε denotes the area fraction (assumed to be equal to the volume fraction) of the carbon particles, bulk solution, SDL and Stern layers. Each flux is reduced due to the resistance R between each phase and the outer electrode.

The dynamic charge transport in the solid bulk carbon (e.g. particles) depends on the local potential gradient and the fluxes from the adjacent Stern layer across the contact surfaces due to micro-, meso- and macro-pores:

$$\frac{dq(x,t)}{dt} = \left[\frac{1}{2}c\frac{1}{(R_C+R_{C\text{-}C})}\frac{\partial\varphi}{\partial x}\right] + \left[\frac{A_{macro}}{R_{Stern\text{-}C}V_{partcile}}J_{q_{Stern,macro}}\right] + \left[\frac{A_{meso}}{R_{Stern\text{-}C}V_{particle}}J_{q_{Stern,meso}}\right] + \left[\frac{A_{micro}}{R_{Stern\text{-}C}V_{particle}}J_{q_{Stern,micro}}\right] \quad (6)$$

where contact resistance $R_{C\text{-}C}$ is considered between carbon particles and resistance R_c is considered within each particle. Figure 8(a) presents a schematic with all these resistances associated with carbon particles.

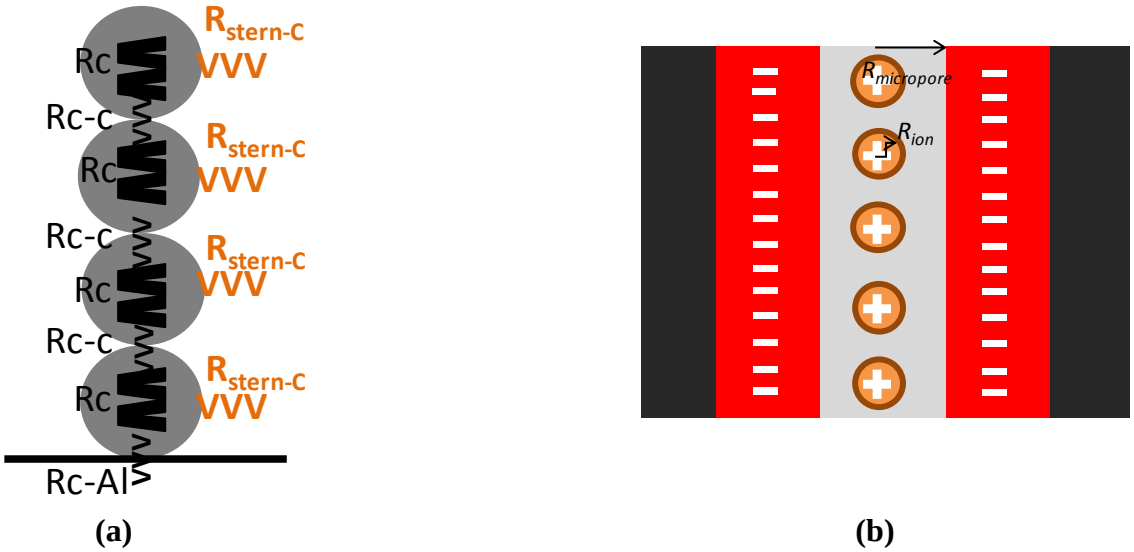

Figure 8. Schematic diagram illustrating (a) the resistances associated with carbon particles, (b) ion transport in a micro-pore

The next stage is to model charge transport inside the pores. Micro-pores have only the Stern layer and their surface is considered cylindrical:

$$\frac{dq(x,t)}{dt} = \left[c\frac{1}{rR_{Stern}}\frac{\partial\varphi}{\partial x}\right] - \left[\frac{A_{micro}}{R_{Stern-c}V_{partcile}}J_q{}_{Stern,micro}\right] + \left[\frac{A_{micro}}{R_{Stern-c}V_{particle}}J_q{}_{SDL}\right] \quad (7)$$

A meso-pore has two layers, the Stern layer and the SDL layer, with a transient equation for the charge transport in each layer in cylindrical coordinates. A macro-pore has three layers, the Stern layer, the SDL layer and the bulk solution layer with a transient equation for the charge transport in each layer, this time in Cartesian coordinates with flat interfaces. Apart from the charge transport equations, there are also mass transport equations that provide the ion concentration as a function of position and time. A solution of the system of equations can be carried out by giving known voltage boundary conditions at the outer electrodes from the cyclic voltammetry tests (for example Figure 6), to predict charge as a function of position and time, which can subsequently translated to capacitance, whereas flow of charge can be related to current.

5. Conclusions

A comprehensive ion transport model has been developed that calculates ion transport and adsorption in micro-, meso- and macro-pores under both steady state and dynamic conditions. Under steady state conditions, the capacitance can be determined in a straightforward manner for all three types of pores, where: effective micro-pore size lies between the minimum size required so that the ions can infiltrate and the maximum size so that the pore has only the Stern layer; meso-pore size is such that the pore has both Stern and SDL layers, whereas macro-pore has these two layers and also the bulk solution, and is considered to have flat interface with the electrolyte.

Preliminary predictions based on steady state charge transport agree with the experimental results for low frequencies and DC. For higher frequency and charge-discharge at various rates a dynamic model is required and the basic concept of such a model has been presented.

Acknowledgements

The authors would like to acknowledge the funding by the European Community under the umbrella of the FP7 Green Cars programme.

References

[1] Biesheuvel P.M., Fu Y., Bazant M.Z. Diffuse charge and Faradaic reactions in porous electrodes. *Physical Review E*, **83**, 061507(6pp) (2011).
[2] Biesheuvel P.M., Bazant M.Z. Nonlinear dynamics of capacitive charging and desalination by porous electrodes. *Physical Review E*, **81**, 031502(12pp) (2010).
[3] Stigter D. Micelle formation by ionic surfactants. III. Model of Stern layer, ion distribution, and potential fluctuations. *J.Phys.Chem.*, **79**(10), pp.1008-1014 (1975).
[4] Huang J., Sumpter B.G., Meunier V. A universal model for nanoporous carbon supercapacitors applicable to diverse pore regimes, carbon materials, and electrolytes. *Chemistry*, **14**(22), pp.6614-6626 (2008).
[5] Lazzari M. *Electrode Materials for Ionic Liquid Based-Supercapacitors*. PhD Thesis, Univ. Bologna (2010).